Supplement of Biogeosciences, 17, 4281–4295, 2020
https://doi.org/10.5194/bg-17-4281-2020-supplement

Biogeosciences Open Access EGU

Supplement of

Seasonal dynamics of the COS and CO_2 exchange of a managed temperate grassland

Felix M. Spielmann et al.

Correspondence to: Georg Wohlfahrt (georg.wohlfahrt@uibk.ac.at)

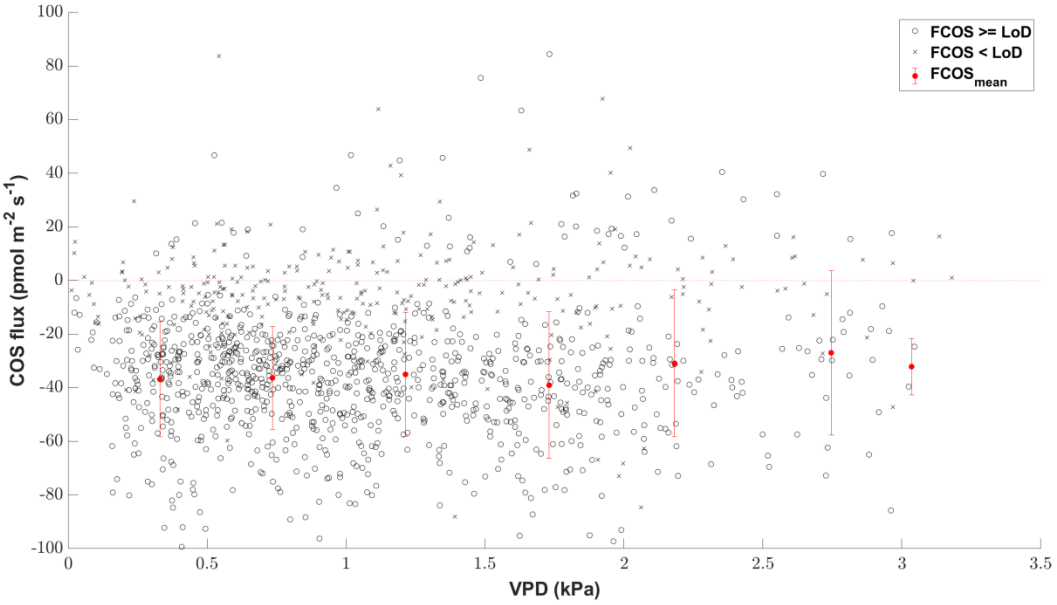

Figure S1 Influence of vapor pressure deficit (VPD) on COS ecosystem flux (pmol $m^{-2}s^{-1}$) at times of high incoming photosynthetic active radiation (PAR_{inc} >= 800 µmol m^{-2} s^{-1}). Black circles depict the COS ecosystem fluxes (pmol $m^{-2}s^{-1}$) if they are above the limit of detection and black x's if they are below. Filled red circles depict the mean COS ecosystem fluxes for VPD of 0.5 (kPa) bins. The red error bars depict the ±1 standard deviation of the mean.

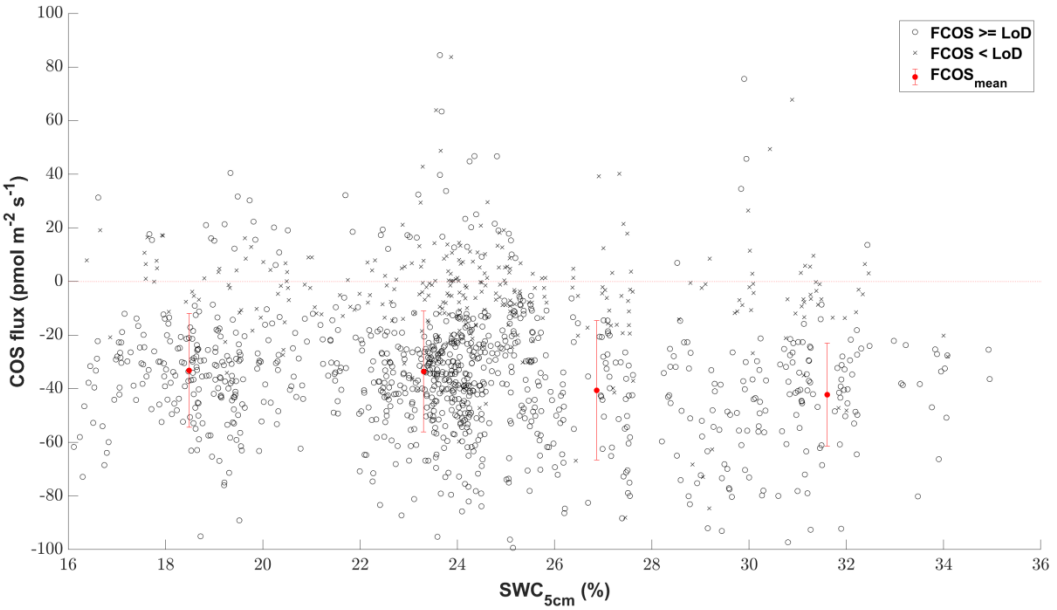

Figure S2 Influence of the soil water content at 5 cm depth on the COS ecosystem flux at times of high incoming photosynthetic active radiation (PAR_{inc} >= 800 µmol m^{-2} s^{-1}). Black circles depict the COS ecosystem fluxes (pmol $m^{-2}s^{-1}$) if they are above the

limit of detection and black x's if they are below. Filled red circles depict the mean COS ecosystem fluxes for SWC_{5cm} of 5 % bins. The red error bars depict the ±1 standard deviation of the mean.

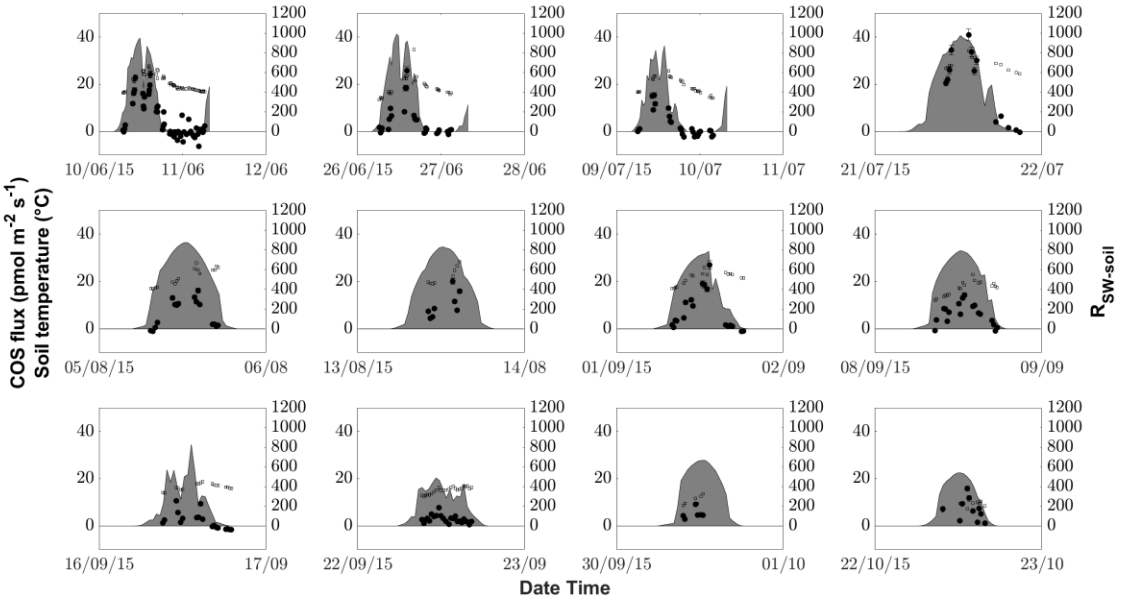

Figure S3 COS and CO_2 soil fluxes (pmol $m^{-2}s^{-1}$ and µmol $m^{-2}s^{-1}$) originating from manual chamber measurements depicted by black circles and diamonds, respectively, incident shortwave radiation reaching the soil surface ($R_{SW\text{-}soil}$) depicted by the gray area and soil temperature (T_{soil}) depicted by empty black bordered squares.

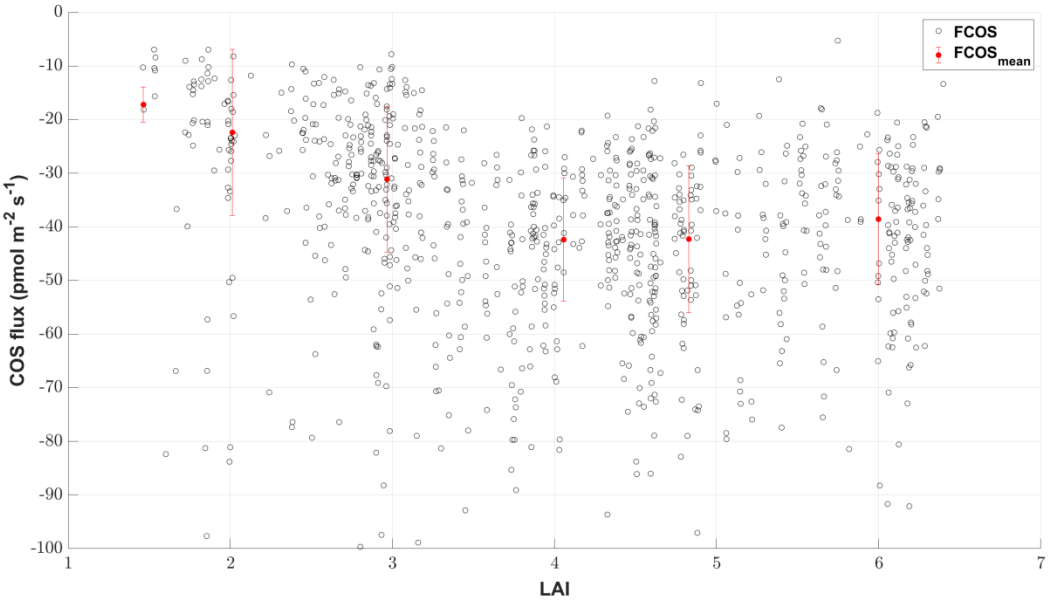

Figure S4 Back circles depict the COS uptake (pmol $m^{-2}s^{-1}$) plotted against the leaf area index (LAI) at times of high incoming photosynthetic active radiation (PAR_{inc} >= 800 µmol m^{-2} s^{-1}), while red filled circles depict the mean COS uptake per LAI class.

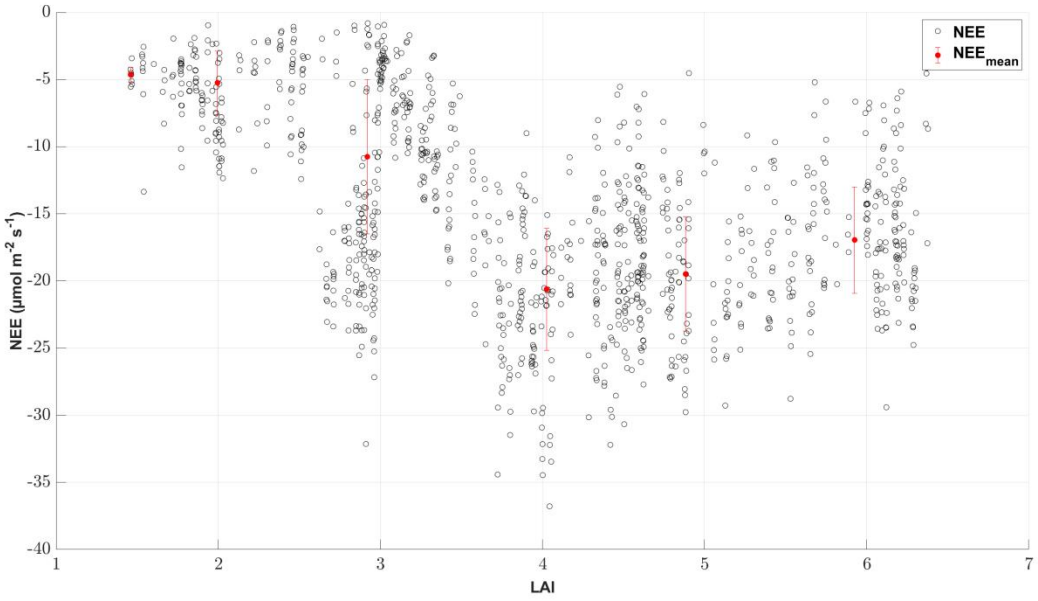

Figure S5 Black circles depict the NEE (µmol $m^{-2}s^{-1}$) plotted against the leaf area index (LAI) at times of high incoming photosynthetic active radiation (PAR_{inc} >= 800 µmol m^{-2} s^{-1}) and filtered to exclude net emissions, while red filled circles depict the mean NEE per LAI class.

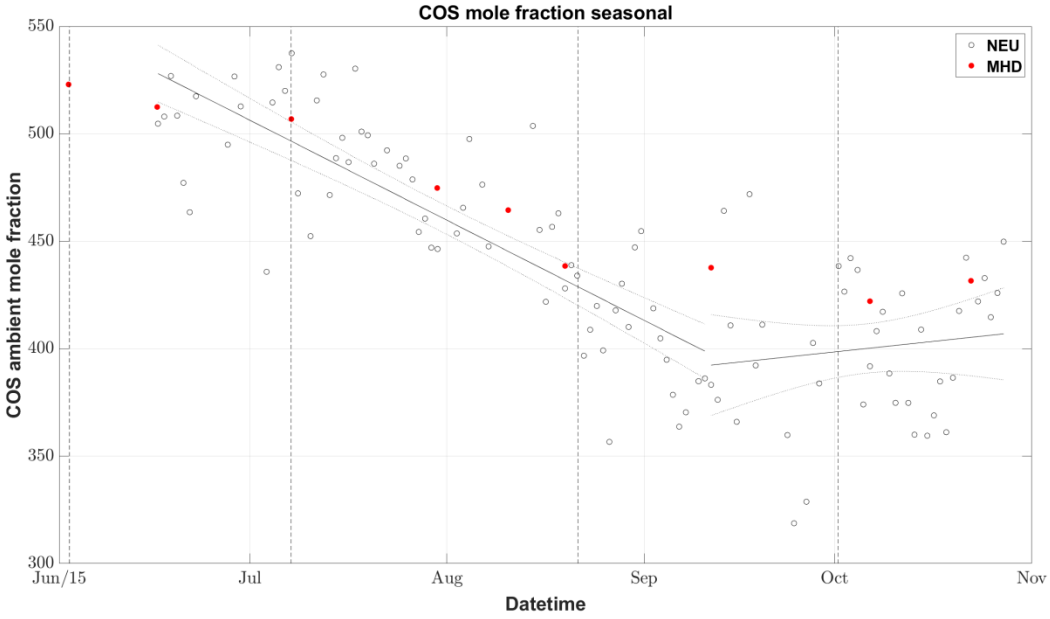

Figure S6 Seasonal COS mole fraction of Neustift (Austria) and Mace Head (Ireland), depicted by black and filled red circles respectively (change point detection Barr et al. (2013)).

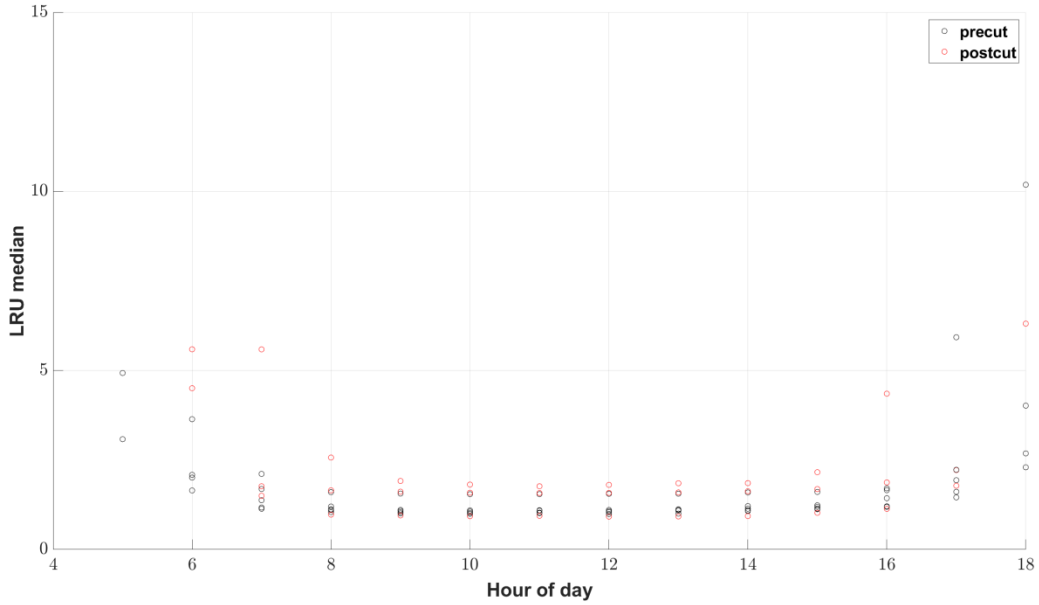

Figure S7 Mean diurnal variation of LRU calculated from ι and κ separated into the pre- and post- cut periods (~15 days each) depicted by black and red circles respectively.

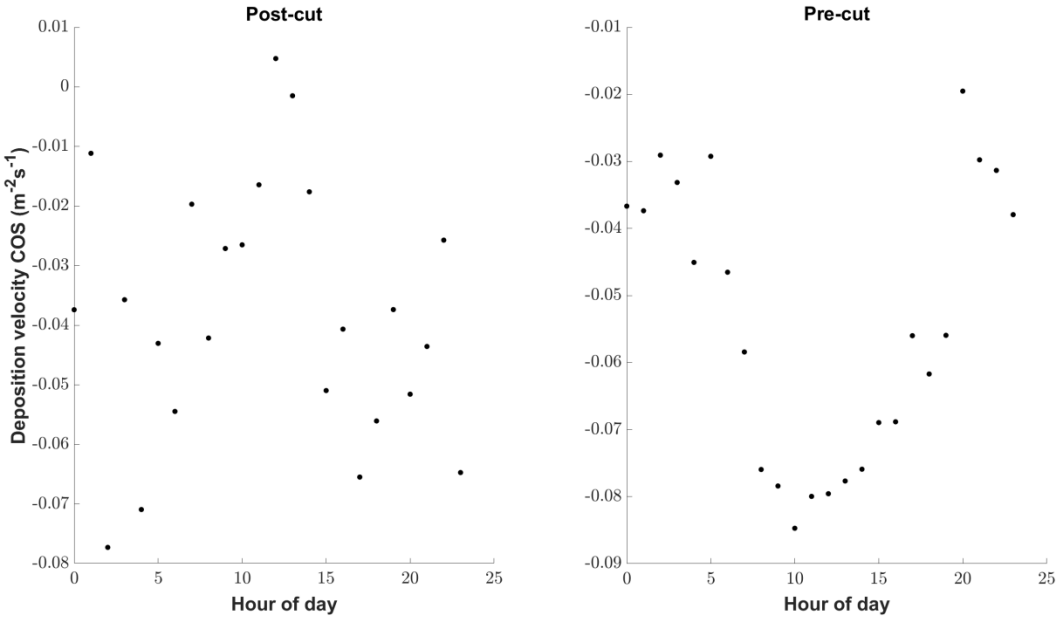

Figure S8 Mean diurnal variation of the COS deposition velocity for low LAI (<=3) and high LAI (>= 4) from May to August.

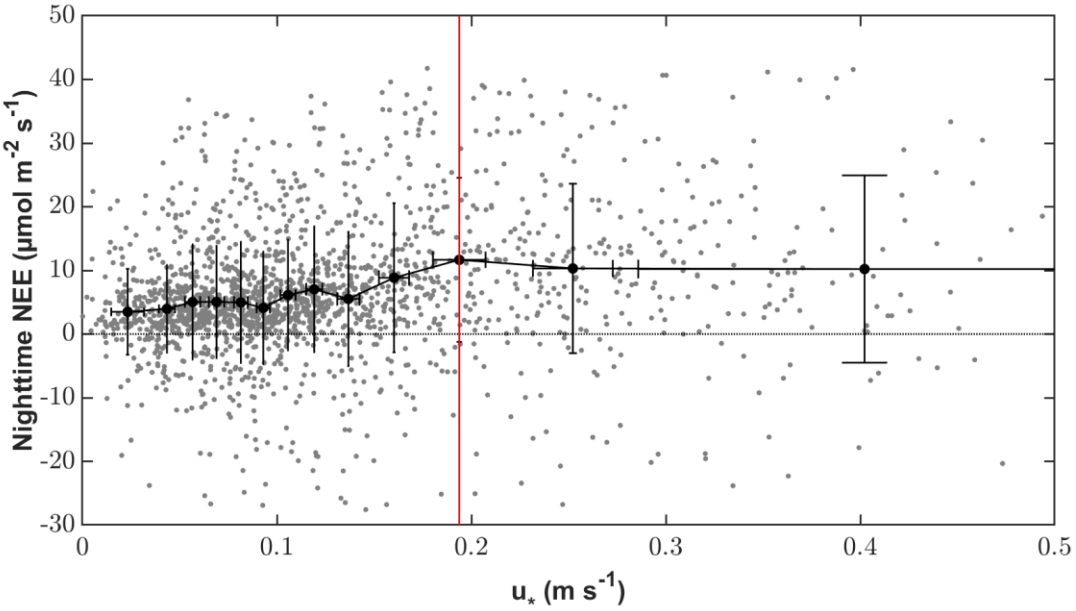

Figure S9 Determination of the friction velocity (u*) threshold for CO_2.

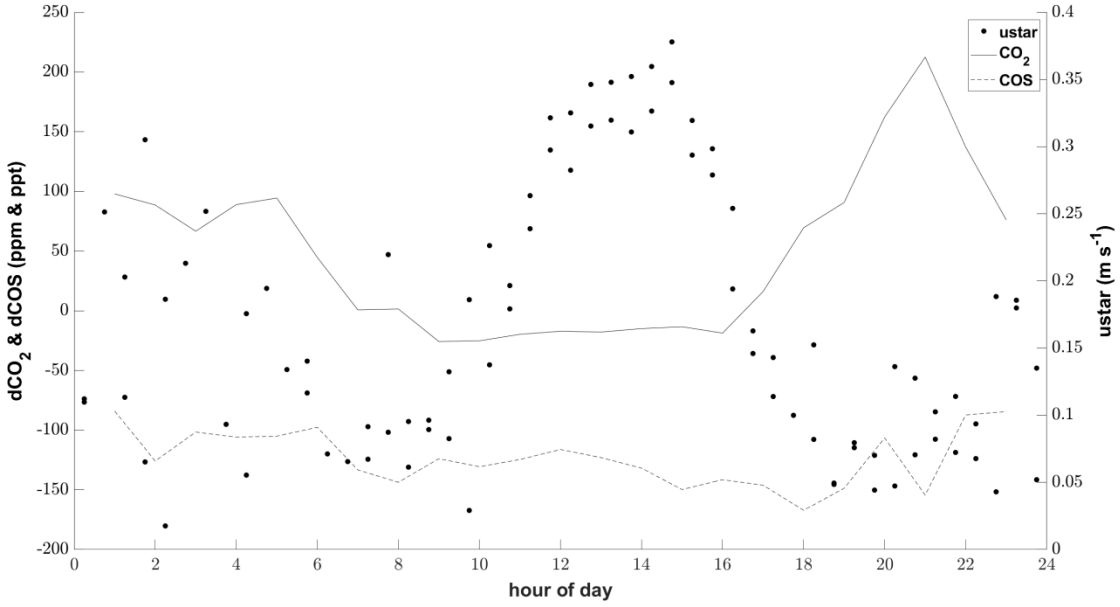

Figure S10 Mean diurnal variation of the difference in mole fractions between the canopy height at 0.4m and 0.02 m or 0.1 for COS (black dashed line) and CO_2 (black solid line) respectively. The black dots depict the friction velocity (ustar). The two lowest measurement heights were excluded for CO_2 since the CO2 mole fraction increased due to the soil respiration.

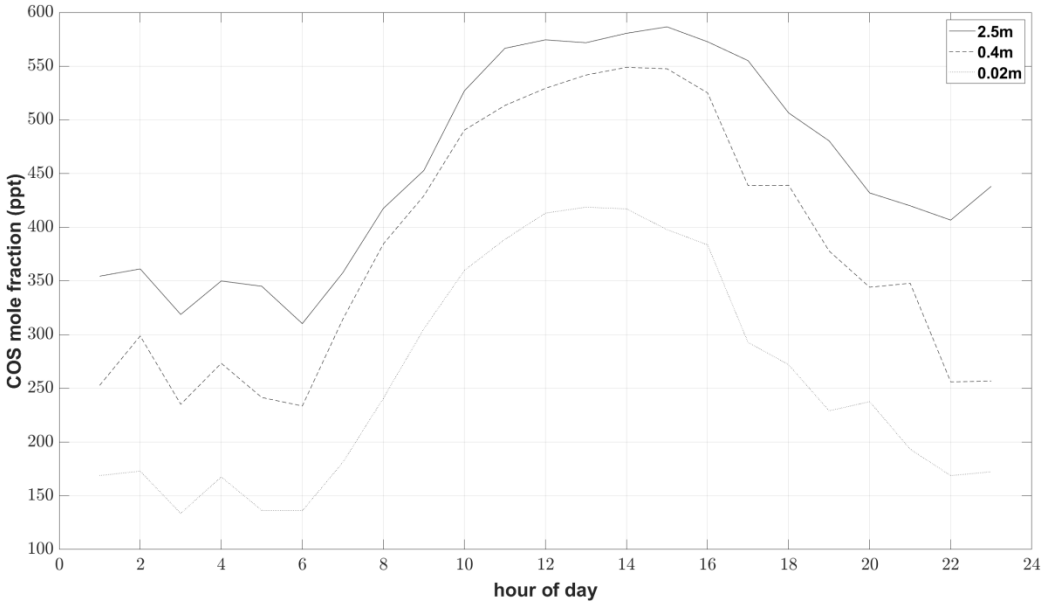

Figure S11 Mean diurnal variation of the COS mole fractions at tower (2.5m), canopy (0.4m) and the lowest measurement height (0.02m).

Photo S1 Grassland before the cut (21.08.2015 12:00)

Photo S2 Grassland during the cut when the grass was left to dry (21.08.2015 16:00)

Photo S3 Dead plant parts covering the majority of the grassland (23.08.2015 12:00)